Impact of Biomass Burning Aerosols on the Diurnal Cycle of Convective Clouds and Precipitation Over a Tropical Island

Alma Hodzic, Jean Philippe Duvel

AGU PUBLICATIONS

JGR

Journal of Geophysical Research: Atmospheres

RESEARCH ARTICLE
10.1002/2017JD027521

Key Points:
- WRF-Chem with aerosol-aware microphysics is used to study effects of fire aerosols on the diurnal evolution of deep convection over Borneo
- Microphysical and radiative aerosol effects are regionally variable and perturb mostly the nighttime convection
- Aerosol absorption modulates the radiative effect by changing the atmospheric heating over the island and the low-level moisture convergence

Supporting Information:
- Supporting Information S1
- Figure S1
- Figure S2
- Figure S3
- Figure S4

Correspondence to:
A. Hodzic,
alma@ucar.edu

Citation:
Hodzic, A., & Duvel, J. P. (2018). Impact of biomass burning aerosols on the diurnal cycle of convective clouds and precipitation over a tropical island. *Journal of Geophysical Research: Atmospheres*, *123*, 1017–1036. https://doi.org/10.1002/2017JD027521

Received 27 JUL 2017
Accepted 19 DEC 2017
Accepted article online 21 DEC 2017
Published online 17 JAN 2018

Impact of Biomass Burning Aerosols on the Diurnal Cycle of Convective Clouds and Precipitation Over a Tropical Island

Alma Hodzic[1] **and Jean Philippe Duvel**[2]

[1]National Center for Atmospheric Research, Boulder, CO, USA, [2]CNRS, LMD, Paris, France

Abstract A coupled weather-aerosol model is used to study the effect of biomass burning aerosols on deep convection over the Borneo Island and surrounding oceans. Simulations are performed at the convection-permitting scale (4 km) for 40 days during the boreal summer and include interactive fire emissions and the aerosol effect on radiative and microphysical processes. Intense burning occurs daily in the southern part of the island, and smoke propagates northward to regions of deep convection. The model captures well the observed diurnal cycle of precipitation and high cloud cover. Cloud microphysics and radiative aerosol impacts are considered separately. Modifications of the cloud microphysics by smoke aerosols reinforce deep convection near the central Borneo mountainous region. This reinforced convection is due to reduced shallow precipitation in the afternoon that leads to a warm planetary boundary layer anomaly at sunset enhancing deep convection at night. Aerosol absorptive properties strongly affect local and synoptic atmospheric responses. The radiative processes of moderately absorbing aerosols tend to reduce deep convection over most regions due to local surface cooling and atmosphere warming that increase the static stability. For more absorbing aerosols, however, the impact is reversed with increased nighttime convection over most regions. This is partly related to changes in the vertical water vapor divergence profiles that decrease the convergence toward Borneo for moderately absorbing aerosols and increase it for more absorbing ones. These changes in the synoptic circulation due to large-scale aerosol perturbations are as important as local processes to explain the observed rainfall perturbation patterns.

1. Introduction

Forest fires and agricultural burning contribute ~30–40% of the global carbonaceous aerosol loading worldwide (Smith & Bond, 2014), and the majority of these emissions (>80%) occurs in the tropics where the convective activity is the strongest. The resulting smoke aerosols have been observed to substantially alter the convective activity and precipitation (Andreae et al., 2004; Rosenfeld, 1999).

These interactions proceed through a complex superposition of radiative and microphysical processes, which are not fully understood, especially within the context of diurnally varying atmospheric parameters (Boucher et al., 2013). Smoke aerosols consist mainly of organic (50–70%) and black (5–15%) carbon (Reid et al., 2005) that both scatter and absorb solar radiation. This direct aerosol radiative forcing cools the surface and warms the atmosphere near the aerosol layer (Yu et al., 2002) and may thus affect low-level cloud formation as well as the convective stability. In addition, smoke aerosols are water soluble and provide additional surfaces for cloud water condensation (Janhall et al., 2010; Petters et al., 2009), which modifies the number of cloud condensation nuclei (CCN) and thus the cloud microphysics. In the lower troposphere, the presence of smoke aerosols typically leads to smaller effective cloud droplet sizes, reduced coalescence, and warm rain precipitation (Albrecht, 1989), and brighter and more persistent clouds (Twomey, 1977). The effect of aerosols on deep convection and high cloudiness is more complex and debatable. One hypothesis is that aerosols may increase the cloud droplet freezing in the convective updrafts releasing more latent heat which could cause stronger updrafts, more precipitation, and larger high cloud cover (Rosenfeld et al., 2008). However, Fan et al. (2013) suggested that the observed increase in high cloud cover could also be due to the formation of smaller ice particles in aerosol-rich environments leading to reduced fall velocities of ice particles and to more persistent high clouds. The relative importance of the radiative and the microphysical aerosol processes on clouds largely depends on the initial aerosol loading and the cloud cover type. Koren et al. (2008) showed that scattered shallow clouds are mostly dissipated by aerosol radiative warming regardless of the aerosol amount, whereas thicker medium- and high-level clouds are invigorated by aerosol microphysical process,

especially at lower aerosol loading. Similarly, Ten Hoeve et al. (2012) showed that increasing aerosol concentrations have the tendency to decrease cloud optical depth in already polluted conditions due to radiative processes and to increase cloud optical depth in clean conditions due to microphysical processes.

One may expect that these tendencies are strongly modulated by the diurnal solar forcing with possible nonlinear responses. To our knowledge, only a few regional modeling studies have analyzed the perturbations caused by smoke aerosols on the diurnal development of clouds and precipitation in the tropics. Using a coarse regional model (60 km resolution) with prescribed monthly mean aerosols over the Amazon, Zhang et al. (2008) showed that the smoke-induced reduction in solar radiation at the surface was partly offset in the early afternoon by the cloud dissipation due to the absorption of the solar radiation by aerosols. This resulted in a maximum aerosol impact on surface fluxes in the late morning. Using somewhat higher horizontal resolution (20 km grid) model with explicit aerosol-cloud microphysics over the Amazon, Ten Hoeve et al. (2012) found that aerosol microphysical processes increase the cloud fraction and optical depth during nighttime, but that radiative processes decrease the cloud fraction during daytime. This perturbation of the cloudiness, that may be attributed mostly to low- and middle-level clouds, possibly feedbacks on the deep convection by modifying the surface radiation budget and the diurnal variation of the surface and planetary boundary layer (PBL) temperatures.

Wu et al. (2011) analyzed more specifically the diurnal variation of deep convection and rain, with an 8 day simulation from the Weather Research and Forecasting with online Chemistry (WRF-Chem) model over South America (36 km and 4 km grid). They reported that radiative processes of smoke aerosols reduced the diurnal amplitude of deep convection, characterized by an afternoon decrease of deep convection that is larger than its nighttime increase. The study by Zhao et al. (2011) showed that dust aerosols have a similar radiative impact on precipitation over West Africa. However, the microphysical effect may induce other feedbacks on the diurnal rainfall modulation in certain large-scale conditions. For instance, Fan et al. (2015) showed a case where the pollution aerosols caused retention of water in the boundary layer during the day that acted as a reservoir of water for the development of larger convection and precipitation over mountainous areas during the night. There is also an induced dynamical impact of aerosols on the convective activity. Zhang et al. (2008) and Ge et al. (2014) reported that daytime aerosol radiative perturbation generates heating contrast between regions of high and low aerosol loadings that may result in dynamical feedbacks on the low-level moisture convergence. Zhao et al. (2011) also observed the diurnal perturbations of the low-level wind over West Africa due to diurnal changes of the boundary layer stability related to radiative effects of dust aerosols.

The goal of this study is to quantify the role of smoke aerosols on clouds and precipitation over Borneo by using cloud-permitting monthlong model simulations with an explicit cloud-aerosol-radiation representation. Our approach is to focus on the diurnal cycle to understand the physical origin of the impact of aerosol on moist processes. The Borneo Island is a suitable location for such an approach as it provides a confined framework where fire aerosol emissions and convective activity are interacting at the diurnal timescale. This gives many similar diurnal occurrences (Yang & Slingo, 2001) that increase the statistical robustness of the results. All aerosol processes mentioned above are susceptible to impact the diurnal cycle and the daily mean cloudiness, precipitation, and circulation over the island and will be analyzed and discussed. This paper is organized as follows: in section 2 modeling framework is described; in section 3 the model results are qualitatively evaluated with satellite measurements for aerosols, high cloudiness, and precipitation; in section 4, the effect of smoke aerosols on convective clouds and precipitation and their sensitivity to aerosol absorption are analyzed; and in section 5, the local and synoptic origins for these perturbations are discussed.

2. Modeling Approach

2.1. Online Chemistry-Transport Model

The simulations of aerosol-cloud interactions were performed using the WRF-Chem model (version 3.6.1), with the aerosol-aware microphysics parameterization of Thompson and Eidhammer (2014). The model was configured using two domains with the outer domain (93°E–132°E and 15°S–15°N) of 20 km grid spacing and the cloud-permitting domain (108°E–120°E and 4.5°S–7°N; see Figure 1) of 4 km grid spacing. Meteorological initial and boundary conditions were obtained from NCEP reanalysis (National Center for

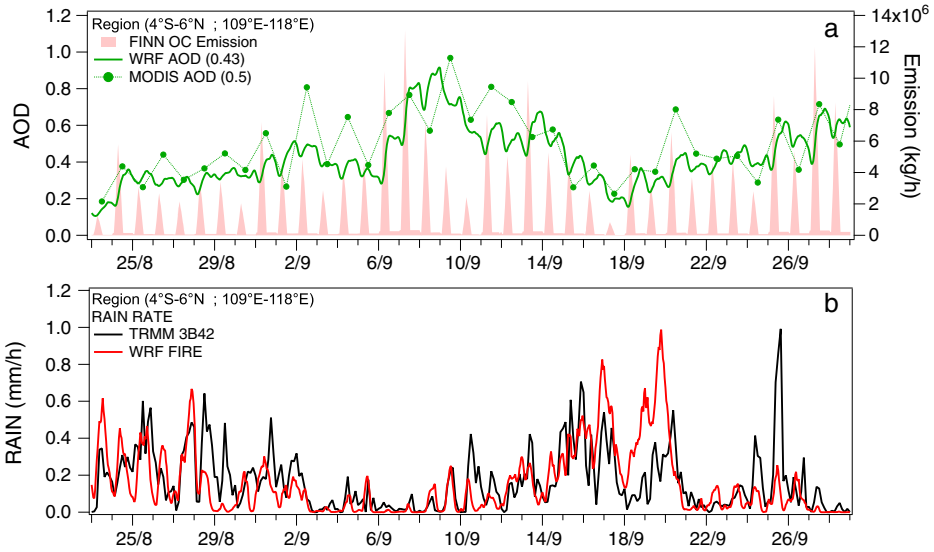

Figure 1. (top) Time evolution of the domain-averaged fire emissions of organic carbon (OC, kg/h) from the FINN inventory, as well as the AOD observed by MODIS and predicted in the FIRE simulation (bottom) rain rates observed by TRMM and predicted in the FIRE simulation.

Environmental Prediction, 2000). WRF-Chem includes many choices of physical parameterizations. Our configuration includes the Rapid Radiative Transfer Model for GCMs (RRTMG) longwave radiation (Iacono et al., 2000), Mellor-Yamada-Janjic boundary layer (Janjić, 2002), and Noah land surface model (Barlage et al., 2010). The Grell and Freitas (2014) cumulus scheme was used for the coarse domain, and no convective parameterization was used for the 4 km domain. The outer domain was nudged to the NCEP reanalysis that has a frequency of 6 h, whereas the inner domain was free running.

The Thompson and Eidhammer (2014) microphysics scheme is a double-moment bulk microphysical parameterization that explicitly treats the activation of aerosols as cloud condensation (CCN) and ice nuclei. Two types of aerosols are included: the hygroscopic aerosol called "water friendly aerosol" (sulfate, organics, and sea salt) and the nonhygroscopic ice-nucleating aerosol called "ice friendly" (mineral dust) aerosols. Cloud droplets nucleation is determined from number concentration of water friendly aerosols using a look-up table of activated fraction, whereas the ice crystals nucleation is determined following the parameterization of DeMott et al. (2010) for condensation and immersion freezing processes and the parameterization of Phillips et al. (2008) for deposition nucleation. In addition to two aerosol species, the scheme also treats five water species including cloud water, cloud ice, snow, graupel, and rain. Aerosols are treated using the simplified WRF-Chem framework as done in Saide et al. (2016). Primary aerosol emissions from anthropogenic sources, fires, dust, and sea salt are considered, and the corresponding aerosol number concentrations needed by the microphysics scheme are determined using the WRF-Chem emission routines. Anthropogenic emissions are from the REanalysis of the TROpospheric chemical composition inventory (Schultz et al., 2007). Biomass burning emissions are based on the Fire Inventory from NCAR (FINN, Wiedinmyer et al., 2011) and were distributed using the online plume rise model (Grell et al., 2011). These emissions have a diurnal cycle, with maximum values at 15 local standard time (LST), which is important to consider to obtain a realistic diurnal variation of the aerosol optical thickness (Hodzic et al., 2007; Wang et al., 2006). Sea salt and dust emissions are calculated online based on meteorological parameters. The chemical production of aerosols is not included in this simplified model version, which does not include gas phase chemical mechanisms and aerosol chemistry. This omission is not expected to substantially affect aerosol number concentrations as the chemically produced aerosols are expected to condense on preexisting particles. To somewhat compensate for the missing production of secondary species (sulfate and secondary organic aerosols), we have tripled the anthropogenic emissions of primary organic aerosols (assuming that secondary organic and inorganic species account for two thirds of the submicron aerosol mass in anthropogenically dominated regions, Zhang et al., 2007). Anthropogenic, fire, and sea salt emissions (except black carbon) are summed up into the total "water friendly" aerosol number concentrations, while the dust emissions are included into the "ice friendly" number concentrations needed by

Table 1
Description of the WRF Sensitivity Simulations

Simulation	FINN fire emissions	Absorption properties[a]	Microphysics	Radiation
FIRE	Yes	Moderately absorbing	Yes	Yes
CLN	No	Moderately absorbing	Yes	Yes
MPHYS	Yes	Moderately absorbing	Yes	No
ABSORB	Yes	Highly absorbing	Yes	Yes
BIS[b]	Yes	Moderately absorbing	Yes	Yes

[a]Based on Ruiz-Arias et al. (2014). Moderately absorbing aerosol corresponds to the "rural type" in Ruiz-Arias et al. (2014) consisting of 70% water soluble and 30% mineral compounds, whereas the highly absorbing aerosol corresponds to the "urban type" and is a mixture of 56% water soluble, 24% mineral, and 20% black carbon aerosols. [b]Modified initial conditions for the zonal wind component that was increased by 1%.

the microphysics scheme. Thus, changes in the fire emissions are expected to only influence the number concentrations of water friendly aerosols. Aerosols are removed by precipitation scavenging based on aerosol collision efficiencies of Wang et al. (2010). Aerosol initial and boundary conditions are taken every 6 h from global simulations of Model for OZone And Related chemical Tracers (Emmons et al., 2010).

Aerosol-radiation interactions are treated within the RRTMG short-wave radiation parameterization (Iacono et al., 2008). Aerosol optical thickness (AOD) is computed at 550 nm from the predicted aerosols. The needed aerosol optical properties such as the spectral aerosol extinction, Angstrom exponent, single-scattering albedo, and asymmetry factor are taken from the parametrization of Ruiz-Arias et al. (2014) based on the predominant aerosol type and relative humidity (RH). Aerosol hygroscopic growth is taken into account assuming the hygroscopicity parameter of 0.4 for water friendly aerosols similar to previous studies (Saide et al., 2016; Thompson & Eidhammer, 2014). This value is based on the work of Petters and Kreidenweis (2007) and is a reasonable assumption for mixtures including a large fraction of organics. This parametrization has been evaluated with the Aerosol Robotic Network (AERONET) data over the United States and found to be suitable for predicting aerosol optical properties from pollution and fire plumes. According to Ruiz-Arias et al. (2014), the single-scattering albedo (SSA) at 440–625 nm ranges from 0.95 (RH of 0%) to 0.99 (RH of 99%) for moderately absorbing aerosols (rural type) and from 0.64 (RH of 0%) to 0.94 (RH of 99%) for highly absorbing ones (urban type). Aerosol absorption properties are highly uncertain for fire aerosols, and typical midvisible SSA values at ambient humidity range from 0.95–0.97 for AERONET sites dominated by boreal forest or peat burning to 0.85–0.9 for sites dominated by grass and shrub burning (Sayer et al., 2014).

2.2. Model Simulations

Five WRF-Chem model simulations are performed for 23 August to 30 September 2009. Their characteristics are summarized in Table 1. All simulations were initialized at 00 UTC 3 days prior to the period of interest (i.e., 20 August 00 UTC) to provide sufficient spin-up period. The base-case simulation (FIRE) includes all the emissions sources and assumes that fire aerosols are moderately absorbing (similar to rural-type aerosols of Ruiz-Arias et al., 2014). The sensitivity simulations are carried out (i) to quantify the overall effect of smoke aerosols on clouds by comparing the reference FIRE simulation with the CLN simulation that does not include biomass burning emissions; (ii) to quantify the radiative effects of smoke aerosols by comparing the FIRE simulation with the MPHYS simulation which only includes aerosol processes on microphysics (aerosols are assumed to be transparent for the radiation schemes) and the microphysical effects of smoke aerosols by comparing MPHYS and CLN; (iii) to assess the role of aerosol composition by comparing the FIRE simulations with moderately absorbing aerosols (rural-type aerosols of Ruiz-Arias et al., 2014) with the ABSORB simulation with highly absorbing aerosols (urban type, Ruiz-Arias et al., 2014); and (iv) to assess the model internal variability compared to aerosol forcing, by comparing the base-case FIRE simulation with a slightly perturbed BIS simulation that is using modified initial conditions for the zonal wind (increased by 1% in both model domains).

2.3. Data Sets and Comparison Methodology

To qualitatively evaluate the distribution of smoke aerosols, we use the MODIS (Moderate Resolution Imaging Spectroradiometer) Level 3 satellite retrievals of AOD at 550 nm at the 1° × 1° horizontal spacing

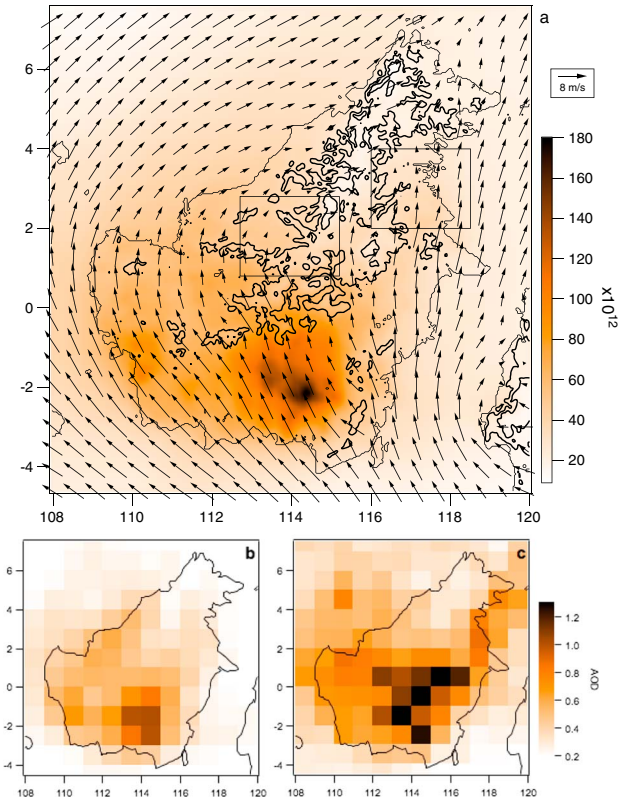

Figure 2. (a) Wind at 440 m above the surface (arrows) and water friendly aerosol number in the column (color in no./m^2) averaged over 23 August to 30 September 2009. (b) AOD as predicted for clear-sky grid points of the FIRE simulation and (c) as observed by the Aqua MODIS satellite at 13:30 LST. The Borneo orography is shown for two levels at 400 m and 1,200 m in Figure 2a.

(used combined dark target and deep blue AOD retrievals from https://giovanni.gsfc.nasa.gov/giovanni/ accessed in January 2017). We use the early afternoon Aqua orbit (13:30 LST) since fire emissions typically peak in the afternoon. One should keep in mind that satellite AOD data could be affected by cloud contamination as discussed in previous studies over this region (Reid et al., 2013). The comparison with the model reference run (FIRE) is performed for AOD averaged for the clear-sky conditions only.

The observed rainfall data used to validate the simulations are Tropical Rainfall Measuring Mission (TRMM) 3B42 (V6) 3-hourly, 0.25° × 0.25° product (Huffman et al., 2007). TRMM tends to underestimate precipitation in regions of intense convection over land, but as noted by Huffman et al. (2007), the overall shape of the rainfall diurnal cycle estimated in TRMM is in a good agreement with observations. We will use TRMM data mostly to evaluate the simulated diurnal variation of the precipitation pattern. The high cloud cover (HCC) is also computed from hourly infrared window channel (10.8 μm) images of the Japanese MTSAT geostationary meteorological satellite with a grid spacing of about 4 km. The HCC is defined as the fraction of grid points having a cloud top equivalent blackbody temperature (EBBT) lower than a given threshold. For observed HCC, the EBBT is derived from infrared window radiance measurements. Since there is no infrared window radiance computed in our WRF simulations, the EBBT is derived from outgoing longwave radiation (OLR) values by simply applying the Stephan-Boltzmann law

$$\mathrm{EBBT} = \left(\frac{\mathrm{OLR}}{\varepsilon\sigma}\right)^{0.25} \quad (1)$$

with the emissivity $\varepsilon = 1$ and $\sigma = 5.67 \times 10^{-8}$ W m^{-2} K^{-4}. For most observations, the OLR gives a smaller EBBT compared to the IR window because of the various absorption bands. However, the difference is small for very high cloudiness and these bands even turn into emission (because of the warmer stratosphere) for cloud tops corresponding to an EBBT lower than 210 K (Duvel & Raberanto, 2000). A threshold of 210 K thus theoretically minimizes the difference between OLR and IR window EBBT. A larger threshold of 230 K is, however, considered in the following to obtain more HCC cases and better cloud statistics. For this threshold, the HCC should be slightly overestimated using the OLR (i.e., in the model) instead of the infrared window.

3. Model Evaluation With Measurements

3.1. Aerosol Distribution

Figure 1a shows the time series of Borneo emissions of organic carbon from fires. During the boreal summer of 2009, smoke emissions occurred almost daily, with the peak fire activity during early afternoon. Some day-to-day variability is observed, with the reduction in fire emissions during rainy days (e.g., between 14 and 24 September). The model captures well the temporal evolution of the corresponding AOD over Borneo and surrounding oceans with maximum values around mid-September. The average rainfall (Figure 1b) presents large day-to-day variations for the period considered with a good general correspondence between the FIRE simulation and TRMM observations. Rainfall maxima occur at the beginning of the simulation and after mid-September and rainfall minima during the first week of September and at the end of the simulation. The aerosol loading is maximal during these dry episodes.

The highest aerosol number concentrations associated with biomass burning are found in the source regions in the southern part of the island (Figure 2a) and are mainly associated with peat and agricultural burning. The freshly emitted smoke is distributed vertically according to the fire size and atmospheric stability using

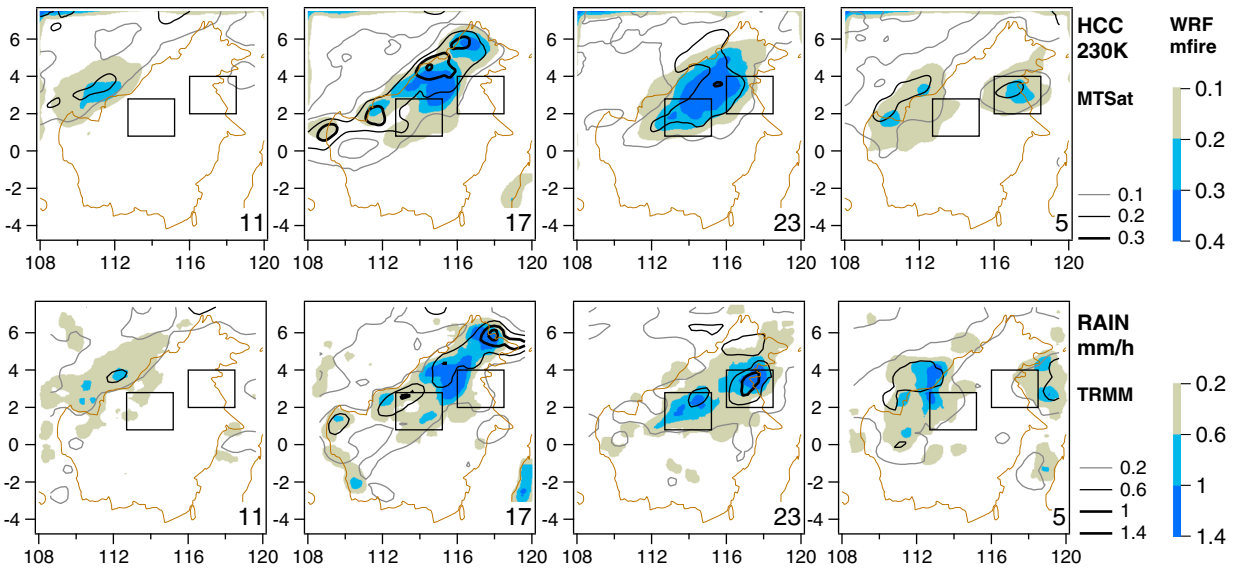

Figure 3. (top row) Average HCC at 230 K between 23 August and 30 September 2009 in the FIRE simulation (colors) and for MTSAT infrared images (contours) for 4 h of the day (in LST). (bottom row) As for top but for average precipitation (mm h^{-1}) in the FIRE simulation (colors) and for TRMM data (contours). Black solid rectangles define the Eastern (North Kalimantan) and the Central (Sarawak) Borneo regions. The fields are smoothed by a box of around 80 × 80 km^2.

the WRF-Chem plume rise module. Most of the smoke is located within the 1.5 km layer above the ground with largest concentrations close to sources (Figure S1 in the supporting information) and is transported within the lower troposphere in the southwesterly flow to the northern shore of the island (Figure 2a). A second much thinner layer of smoke is found between 3 and 5 km above the sea level in the source region. The simulated mean plume heights are consistent with values observed by Tosca et al. (2011) during this period, who reported that 95% of dense smoke plumes were below 1.3 km based on MISR data and that thinner smoke plumes were present between 2 and 4.5 km based on CALIPSO lidar data.

A comparison with the monthly mean MODIS Aqua AOD 550 nm measurements is shown in Figures 2b and 2c. As expected, the modeled AOD in the FIRE simulation is maximal over the fire source region in the southern part of the island (Central Kalimantan). Only a qualitative comparison is performed with MODIS due to likely cloud contamination and calibration issues over this region (Reid et al., 2013). The comparison shows similarities in terms of spatial distribution of smoke; however, the observed AODs are a factor of around 1.3 higher than the predicted values. In addition to cloud contamination, these differences can arise from underpredicted fire emissions as suggested in Kaiser et al. (2012) (by up to 3.5 times) and due to the underestimated growth of organic aerosols by condensation of oxygenated organic gases which is not included in our simulations (though this would not change the aerosol number concentrations). The uncertainties can also arise from the underestimated hygroscopic growth of aerosols. The average nonsmoke (CLN run) AOD is ~0.1 in our study, which is consistent with previous studies (Ge et al., 2014).

3.2. Deep Convection: High Clouds and Precipitation

The representation of the deep convection is first evaluated by comparing the rain predicted by the FIRE simulation, which has the more realistic aerosol configuration, to TRMM observations. The daily average rain rate spatial distribution is in good agreement with TRMM, with maximum convection near the South China Sea (SCS) coast (Figure S2). WRF tends, however, to overestimate the rainfall over the most unstable convective regions and to underestimate it in the adjacent regions, in particular over the SCS to the north and over the western part of Borneo (Figure S3). On average over the simulation, the FIRE simulation gives a domain-averaged rainfall deficit of 0.4 mm d^{-1} compared to TRMM. The rainfall has a strong diurnal cycle that is remarkably well reproduced by the FIRE simulation as shown in Figure 3. The deep convection is initiated at 14 LST over land near the SCS coast and over the orography. It drastically increases with a slight eastward motion between 14 LST and 17 LST. The convective area around 3°N then moves eastward and reaches a maximum over the Eastern (North Kalimantan) Borneo around 23 LST. At the same time, the

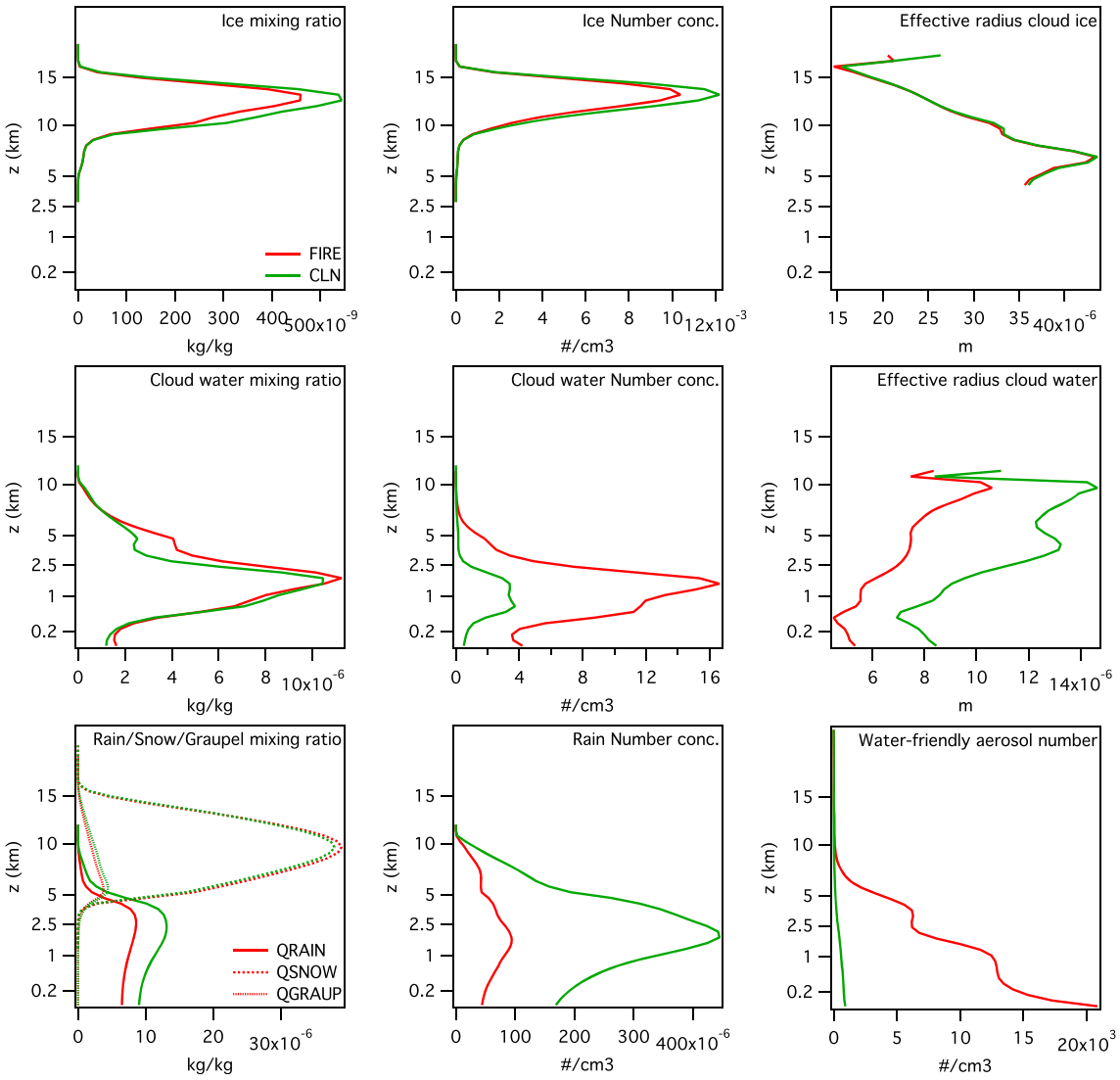

Figure 4. Average profiles of aerosol number concentrations and microphysical parameters over Borneo (4°S to 6°N; 109°E to 118°E) for FIRE and CLN simulations averaged over 23 August to 30 September. Average water and ice cloud droplet sizes are weighted by the droplet number concentration.

convection develops to the south and also reaches a maximum over the Central (Sarawak) Region. After midnight, the northeastern convective perturbation continues to move eastward over the Celebes Sea, while the southwestern convective perturbation moves northwestward over the SCS. In the morning, only the perturbation located over the SCS remains and then dissipates when the convection is triggered inland at 14 LST. As for precipitation, the observed HCC diurnal cycle is well reproduced by WRF (Figure 3), in particular the delayed HCC maximum in regard to rainfall maximum over Eastern Borneo. The HCC pattern is quite similar to the rainfall pattern while much less patchy. HCC fields extend southwesterly more than rainfall because cirrus clouds are advected by the dominant southwesterly winds at these pressure levels.

4. Smoke Aerosol Effects on Convection and Clouds

4.1. Overall Changes in Microphysics Parameters

Figure 4 shows the vertical distribution of average aerosol number concentration and cloud microphysics parameters over the whole Borneo domain for FIRE and CLN simulations. Smoke aerosols dominate the aerosol number concentrations in the lower troposphere, with an average of ~11,000 particles/cm^3 below

5 km in the FIRE simulation compared to ~1,000 particles/cm^3 in the CLN simulation. Although the largest concentrations are found in the boundary layer, a second 3–5 km layer can be seen in the profiles. As expected, the presence of smoke aerosols leads to an increase in number concentrations of cloud droplets (by a factor of 4) in the lower troposphere. These droplets are about 30% to 40% smaller in size in the FIRE run compared to the CLN run. In the FIRE run, the cloud water mixing ratio is slightly decreased at the top of the PBL (1.5 to 2 km) and increased above, which is consistent with the fact that the cloud base is somewhat lifted and that the liquid water content is larger in the presence of smoke aerosols as described below. This cloud water rise (especially large at ~4 km) is likely due to the reduced rainfall that increases the residence time of liquid water in the lower troposphere. Although smoke aerosols are not directly nucleating ice particles, their effect on ice clouds is far from being negligible, partly because of the weaker convective activity in FIRE compared to CLN as shown in the next section. The size of ice particles is unchanged, but an ~20% decrease in their number concentrations and mixing ratios is found for high-level clouds (12–15 km).

As expected, smoke aerosols tend to suppress warm rain, which is clearly seen from the decrease in the rainwater mixing ratio and rain number concentrations. This is related in part to a weaker cloud droplet coalescence described by Albrecht (1989). The graupel mixing ratio is also slightly smaller in FIRE due to weaker deep convective activity compared to CLN. However, the snow mixing ratio is slightly larger in FIRE, possibly due to the upward transport of a larger number of smaller size droplets. It should be noted that compared to the results of previous studies (e.g., Fan et al., 2013 ; Krueger et al., 1995), the graupel mixing ratio seems to be low and the snow mixing ratio seems to be high relative to cloud and rain mixing ratios. This could be due to the presence of large convective anvils over the region. Similar changes are found for MPHYS (not shown) as for FIRE, which indicates that aerosol effect on microphysics dominates the anomalies discussed above.

4.2. Average Microphysical and Radiative Effects

Aerosol effects on convection are quantified from differences between simulations. The difference between FIRE and CLN quantifies the net aerosol effect that may be further separated into aerosol radiative (FIRE-MPHYS) and microphysics (MPHYS-CLN) effects. This distinction only accounts for primary effects including the diminution of the surface solar radiation by aerosols (direct radiative effect) for FIRE-MPHYS or the decrease of warm precipitation due to additional condensation nuclei (microphysical effect) for MPHYS-CLN. The same relative contribution analyses can be performed on the ABSORB sensitivity simulation instead of the reference FIRE simulation.

Figure 5a shows that the differences in daily averaged rain rates among the simulations are relatively small compared to the large day-to-day variability and compared to differences with TRMM observations. For most days, the simulated rain rate is within 30% of the observed values, with the exception of 18–19 and 24–26 September where a factor of 2–3 overprediction and underprediction can be seen, respectively. When integrated over the entire study period and the Borneo domain, the predicted rain rates are reasonably close to TRMM observations (4.1 mm d^{-1}) with a slight overestimation for the CLN simulation (4.3 mm d^{-1}) and underestimation for the FIRE simulation (3.7 mm d^{-1}). The best agreement is obtained for ABSORB and MPHYS with ~4 mm d^{-1}. These results show that the domain-averaged rain rates and its day-to-day variation are mostly controlled by lateral boundary conditions and that the smoke aerosol effect is comparatively small.

The perturbations related to smoke aerosols are better appreciated on the average diurnal cycle of precipitation and anomalies (Figures 5b and 5c), which shows significant differences between the simulations despite the averaging over a large domain. Observed and simulated precipitation have a strong diurnal cycle characterized by a steep increase in the afternoon leading to an evening maximum between 18 and 21 LST. This is followed by a slower decrease overnight and then a steeper decrease during morning hours that results in a precipitation minimum at noon. The largest differences between simulations are found during evening and nighttime hours (18 and 6 LST). The CLN simulation has the most pronounced precipitation peak in the evening, while FIRE is the driest one throughout the day. The ABSORB simulation has a different diurnal evolution shape, which matches closer the TRMM estimates, especially for the slow nighttime decrease. ABSORB gives less rainfall than CLN between noon and midnight, but this is compensated by the larger rainfall during the rest of the day.

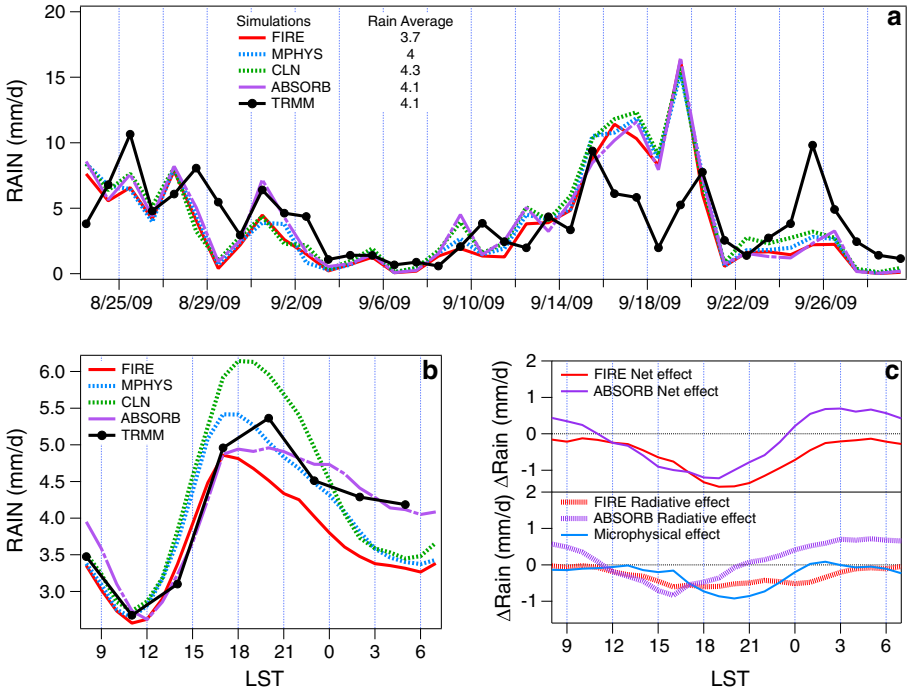

Figure 5. (a) Daily mean and (b) diurnal time series of precipitation averaged over Borneo (4°S to 6°N; 109°E to 118°E) for FIRE, CLN, MPHYS, and ABSORB simulations and for TRMM. (c) Diurnal variation of the aerosol rain perturbation for microphysical effect (MPHYS-CLN), radiative effect for FIRE (FIRE-MPHYS) and ABSORB (ABSORB-MPHYS), and net effect for FIRE (FIRE-CLN) and ABSORB (ABSORB-CLN).

Figure 5c shows that smoke aerosols significantly modulate the diurnal cycle of precipitation with up to ~25% decrease in rain during the afternoon in both FIRE and ABSORB and ~15% increase in rain between midnight and early morning in ABSORB. Since average rainfall rates are nearly identical for all simulations at noon, the significance of the difference between diurnal cycle amplitudes can be estimated considering the average rainfall at the hour of maximum difference. Considering FIRE or ABSORB at 1900 LST, a Student's *t* test gives a difference significant at the 0.99 confidence level compared to CLN. The difference between the diurnal cycles of FIRE and ABSORB is significant with a 0.95 confidence level at midnight. The BIS simulation gives results similar to FIRE (not shown). The relative contribution of radiative and microphysical processes to smoke-related anomalies in surface precipitation is also shown in Figure 5c. The microphysical processes suppress the rainfall at any time of the day with a maximum effect in the evening, that is, during the peak of convective activity over continental regions (Figure 3). The decrease in precipitation due to microphysical processes of smoke aerosols is expected (Albrecht, 1989), although the impact of these microphysical processes on the deep convective rainfall diurnal cycle is unclear at this stage. For mostly scattering aerosols (FIRE), radiative processes further decrease the rainfall between noon and 3 LST and together with microphysical processes reduce the domain average precipitation for all hours. The radiative effect is very different both in amplitude and sign for more absorbing aerosols (ABSORB) with a positive rain perturbation between 21 LST and noon leading to a net rain increase between midnight and noon. This is in a better agreement with the results of Wu et al. (2011) who found a decrease in the rainfall during the day partly compensated by a nighttime increase.

4.3. Distribution and Diurnal Cycle of Microphysical and Radiative Effects

The magnitude, sign, and physical nature of the impact of smoke aerosol on precipitation and high cloudiness show a strong regional variability. As illustrated in Figure 6a, smoke aerosols in the FIRE simulation have mostly a negative effect on precipitation and tend to increase precipitation and HCC only over a southwest-northeast oriented strip parallel to the SCS coast, which corresponds to convectively unstable areas in the afternoon (Figure 3). This positive anomaly strip is flanked north and south by two large negative anomalies. Due to the intermittent nature of precipitation and to the relatively short time series, the rainfall anomaly is

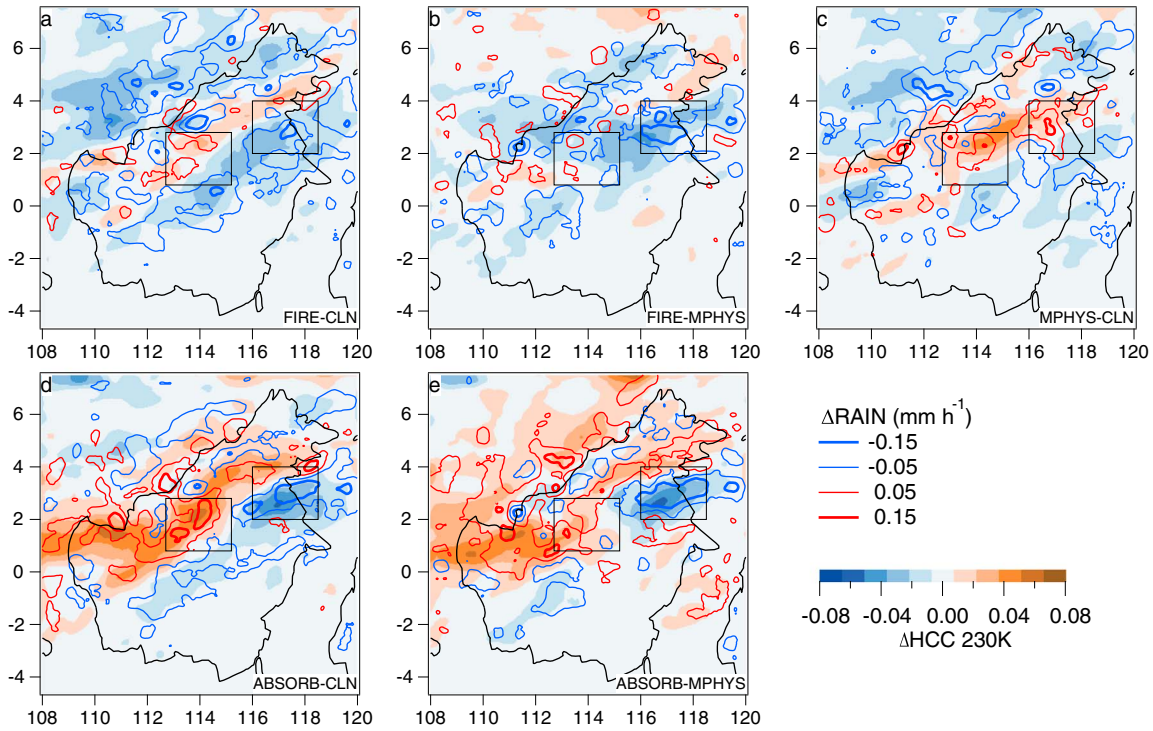

Figure 6. Differences between maps of HCC 230 K (colors) and rainfall (mm h^{-1}, contours) averaged over the whole simulation: total aerosol effect for (a) FIRE and (d) ABSORB, radiative aerosol effect for (b) FIRE and (e) ABSORB, and (c) microphysical aerosol effect. Black solid rectangles define the Eastern and the Central Borneo regions. The fields are smoothed with a 15 × 15 grid point box.

somewhat patchy in the area of positive cloudiness anomaly (e.g., near 3°N–113°E). To determine the significance of these differences between FIRE and CLN in regard to the stochastic noise due to the internal variability of the model, they are compared to the differences between FIRE and BIS. The distribution of FIRE-CLN differences has indeed a larger standard deviation (0.9 compared to 0.7 mm d^{-1}) and is shifted toward negative values (−0.5 compared to −0.04 mm d^{-1}) compared to FIRE-BIS differences. BIS gives in addition similar anomaly patterns compared to FIRE (not shown).

The decomposition into microphysical and radiative aerosol anomalies provides some information on the origin of these regional differences. The two processes tend to act in opposite directions in convective regions where rainfall is reinforced by aerosol microphysical processes by more than 1 mm d^{-1} over large areas (Figure 6c) and is suppressed by comparable amounts by radiative processes (Figure 6b). The modulation of the convection by aerosol microphysical and radiative processes may have various physical origins that will be discussed more specifically for the Eastern and Central Borneo regions outlined in Figures 3, 6, and 7.

With larger aerosol absorption (Figure 6e), convective rainfall is strongly enhanced by aerosol radiative processes over most of northern Borneo and the adjacent ocean, and it is strongly inhibited over eastern Borneo. Note that both precipitation and HCC are slightly reduced by aerosol radiative effect over land along the SCS coast. The rainfall anomaly pattern is roughly similar to that in FIRE (Figure 6b) but with larger magnitude for ABSORB. Over some regions the sign of the rainfall anomaly is, however, reversed, in particular over the SCS. In the ABSORB simulation, the pattern of the net aerosol effect (Figure 6d) is clearly controlled by radiative processes.

The positive rainfall anomaly due to aerosol microphysical processes is mostly due to early morning convection over mountainous terrain and to convection in the afternoon along the SCS coast (Figure 7). Microphysical processes tend to suppress convection over land at night. The large convective inhibition over the Eastern Borneo region is related to nighttime radiative processes in both FIRE and ABSORB. For FIRE, the nighttime radiative enhancement of the convection surpasses the daytime inhibition over a few regions only. For ABSORB, the nighttime radiative enhancement of the convection largely dominates over land, especially

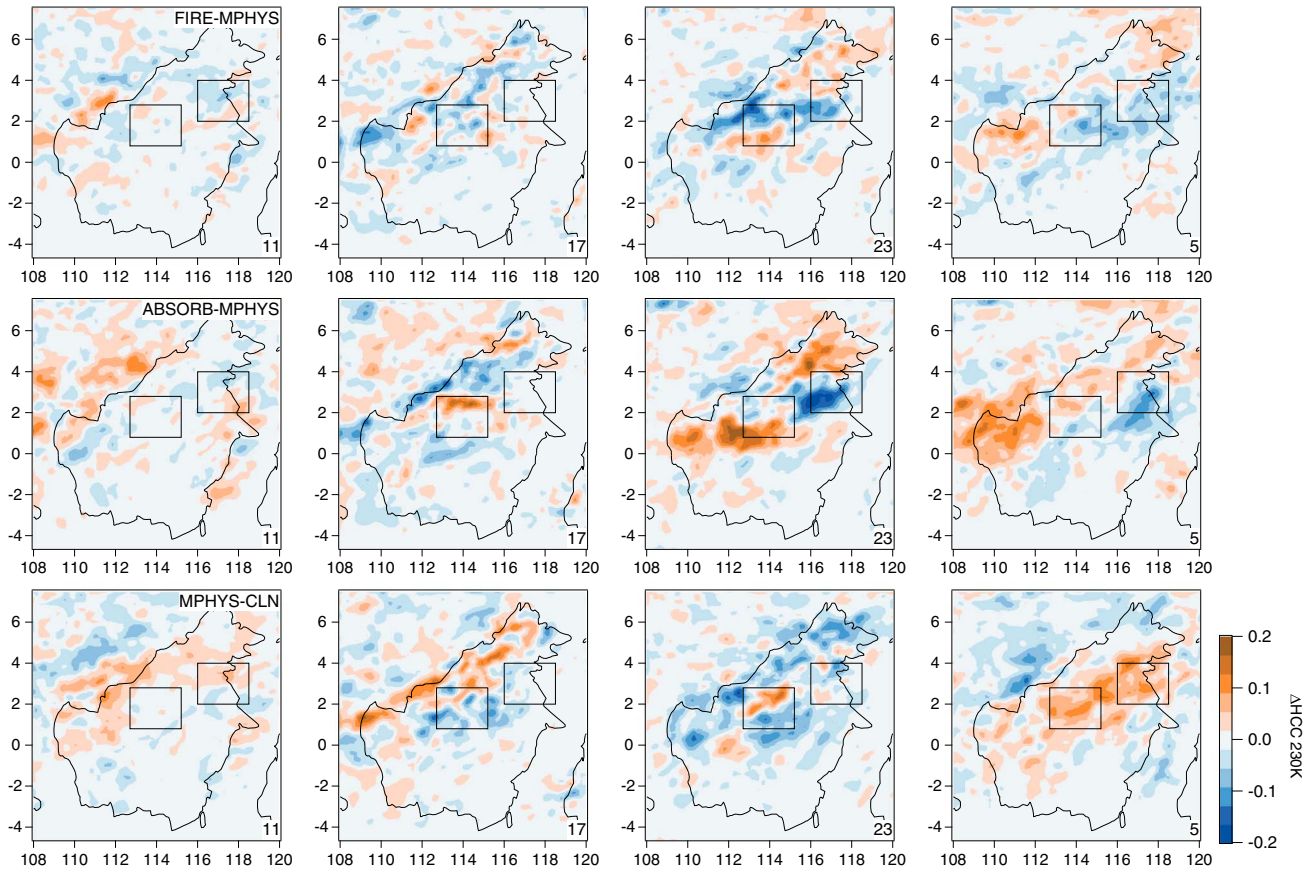

Figure 7. Average difference maps showing the radiative aerosol effect for (top row) FIRE and (middle row) ABSORB and (bottom row) the aerosol microphysical effect on HCC 230 K at four local times. Regions for which HCC are increased by aerosols appear in red. The local times are indicated in the bottom right corner of the maps. Black solid rectangles define the Eastern and the Central Borneo regions.

over western Borneo where the aerosol loading is larger compared to northern regions. The morning rainfall over the SCS is also reinforced by radiative processes in ABSORB.

5. Local and Synoptic Origin of Aerosol-Related Rainfall Anomalies

In the results discussed above, the aerosol perturbation of the diurnal evolution of cloud and rainfall is likely a combination of (i) local aerosol effects involving microphysical and radiative process modifying the static stability of the PBL, the cloud cover, and warm precipitations and (ii) synoptic-scale effects related to large-scale aerosol perturbations of surface and atmospheric temperatures. During daylight hours, the island becomes warmer than the surrounding oceans and generates a depression that reinforces moisture convergence and precipitation on the island. This hot spot effect may be affected by aerosols and by aerosol properties and lead to a significant modification of the diurnal water supply to the island (Ge et al., 2014). Synoptic-scale effects may be dominant over convective regions, including our Eastern and Central Borneo regions, where the aerosol loading is small compared to dry regions farther south.

5.1. Regional Diurnal Rainfall Evolution

The Eastern Borneo region (defined in Figures 3, 6, and 7) is a convective region of low elevation, partly oceanic, where the convection develops late compared to the average diurnal variation over the domain (Figures 3 and 8a). For this region, the model overestimates the rainfall and has an earlier rain maximum compared to TRMM (Figure 8a). Aerosol microphysical processes give a large positive rainfall anomaly during night and a slight negative one in the evening (Figure 8b), causing a delay of about 3 h for maximum rainfall in MPHYS compared to CLN (Figure 8a). Aerosol radiative processes give a strong negative rain and HCC anomaly during night (Figures 7 and 8b) but have little effect during daylight hours. Aerosol microphysical

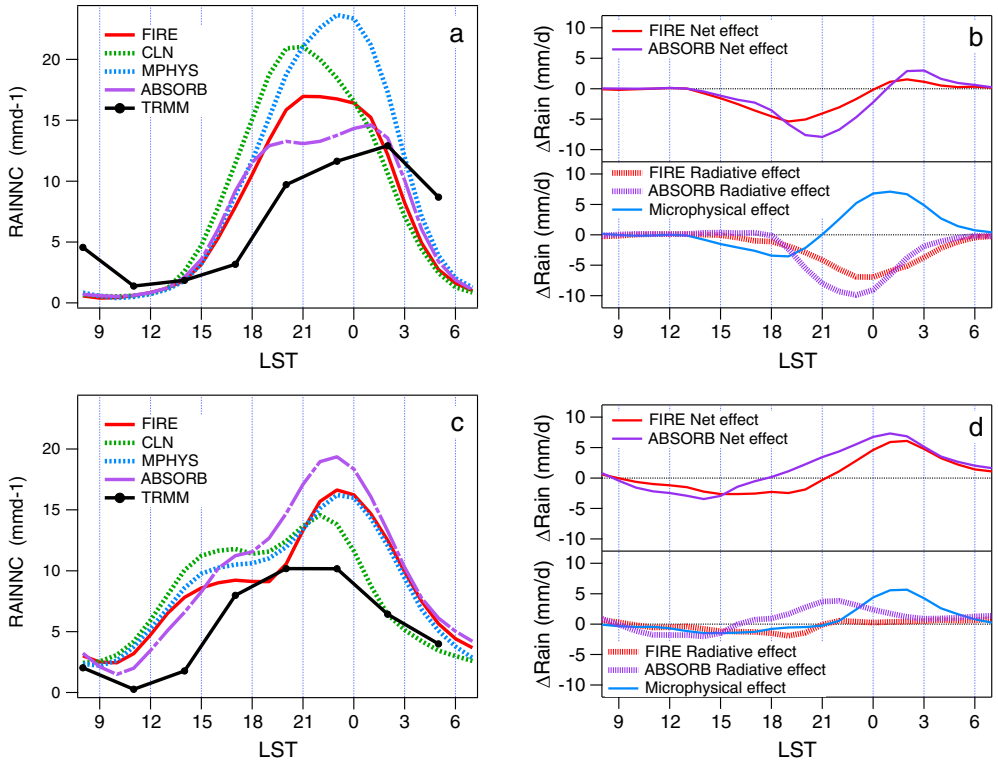

Figure 8. (a) Average rainfall diurnal variation for four simulations and for TRMM observations over the Eastern Region centered on 3°N–117°E. The average diurnal cycle is computed for the entire simulation period (23 August to 30 September). (b) Corresponding average diurnal variation of the aerosol radiative, microphysical, and net perturbations of the average rainfall. (c, d) As in Figures 8a and 8b but for the Central Region centered on 1.8°N–114°E.

processes thus delay the hour of the maximum rainfall, while radiative processes reduce the rainfall with a larger effect for ABSORB compared to FIRE.

The Central Borneo region is another convective region, with mountains to the southwest, where the simulated convection has a double maximum, one around 15 LST (mostly over the orography) and the other around 23 LST (Figure 8c). This region is more affected by fire aerosols compared to Eastern Borneo (Figure 2). For this region, the model also overestimates the rainfall compared to TRMM that has a single rainfall maximum around 21 LST (Figure 8c). As for the Eastern Region, aerosol microphysical processes give a positive rainfall anomaly during night and a small negative one during the day (Figure 8d). The radiative processes give, however, a very different rainfall response with a positive anomaly between 15 LST and 3 LST for ABSORB preceded by a weak negative one around noon and only a very weak radiative perturbation all along the day for FIRE. The diurnal evolutions of the net aerosol impact (Figures 8b and 8d, top) are quite similar for the two regions for FIRE but are quite different for ABSORB because of the very different radiative responses.

5.2. Regional Diurnal Evolution of the Vertical Profiles

The Eastern Region (Figure 9) is characterized by a large diurnal variation of surface temperature (up to 10 K) and PBL height with maximum values near 13 LST. The air temperature has smaller diurnal amplitude from 5 K in the first model level to 1 K at 5 km (Figure 9a) and is maximal between 15 and 18 LST. The maximum rainfall (Figure 8) and upward vertical motion above the PBL (Figure 9a) are reached between 18 and 21 LST, together with the cloud water content peaking at 2.5 km and the ice cloud content peaking at 10 km. After midnight, the convection evolves into a typical stratiform structure with environmental air converging at midlevel and diverging at lower and upper levels (Houze, 1997), giving upward motions above 5 km and subsidence below.

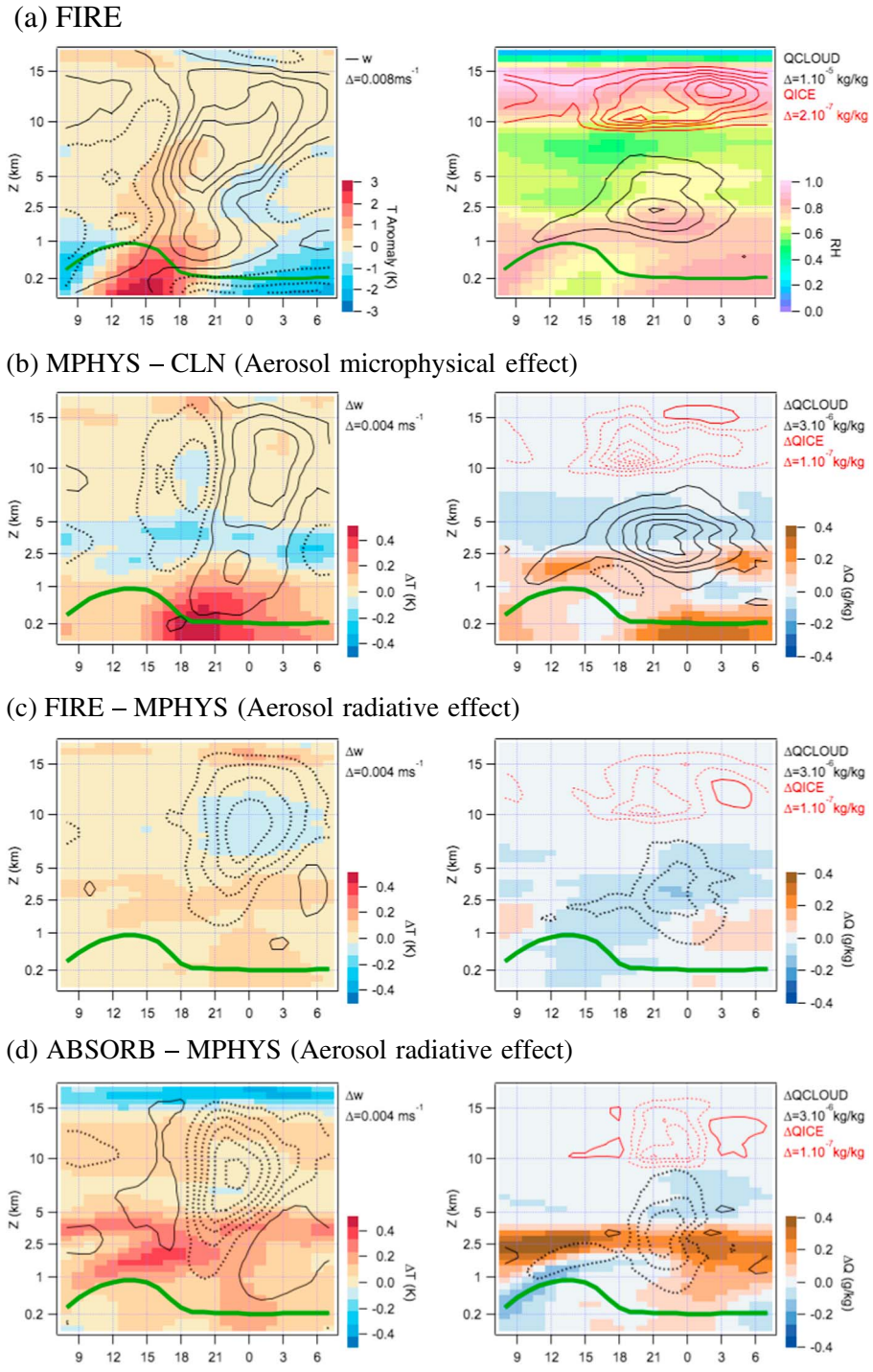

Figure 9. Diurnal evolution of vertical profiles over the Eastern Borneo region (centered on 3°N–117°E) for different parameters for (a) FIRE, (b) MPHYS-CLN, (c) FIRE-MPHYS, and (d) ABSORB-MPHYS. Profiles are averaged on model levels for the entire simulation period (23 August to 30 September). The green curve represents the planetary boundary layer height. In Figure 9a, the temperature anomaly is computed by subtracting the average temperature profile over the region. Negative anomalies are dashed lines. Contour intervals Δ are indicated, and the first contour corresponds to half the interval.

The cloud water content is larger and distributed at higher level (Figure 9b) in MPHYS compared to CLN, as already observed in Figure 4 for FIRE and for the whole domain. This is related to a colder layer between grossly 1 and 5 km. The atmosphere is moister below 2.5 km and drier above. The larger MPHYS cloud cover only slightly modifies the surface insolation (-2.4% or -20 W m^{-2} at noon) and the surface temperature

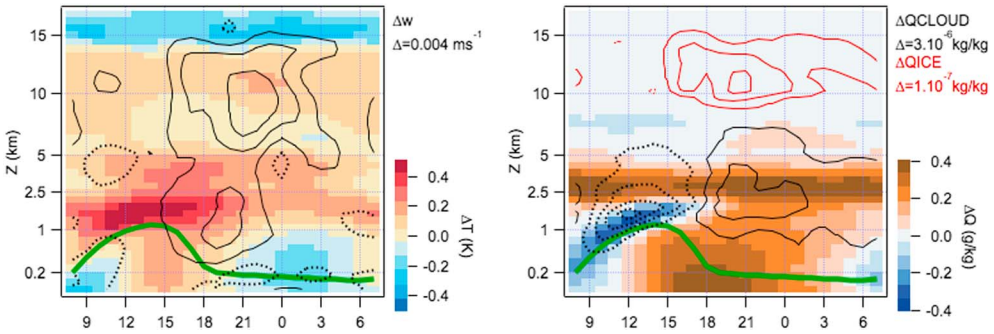

Figure 10. As in Figure 9 but only for ABSORB-MPHYS over the Central Region.

(−0.1 K at noon) and can hardly explain the reduced updraft around 18 LST. The PBL is warmer in MPHYS, but it is also drier between 15 LST and 18 LST, with a reduced cloud water content around 1 km that denotes a higher lifting condensation level and a reduced convective instability. A hypothesis is that the reduced cloud droplet coalescence in MPHYS delays the formation of precipitating shallow convective clouds resulting in (i) a slightly warmer PBL because of smaller rain evaporation in a warming PBL (note the reduced RH for these hours in Figure 9a), (ii) a moister cloud layer (as seen between 1 km and 2.5 km between noon and 15 LST), and (iii) a drier atmosphere above 2.5 km because of the lack of cloud top detrainment. The resulting smaller injection of moisture at upper levels may inhibit deep convection by drying the lateral air entrainment and may thus delay the triggering of the deep convection.

At the end of the afternoon, the PBL is much warmer in MPHYS with maximum temperature anomaly up to 0.5 K at 19 LST (Figure 9b). This warming can be mostly attributed to the precipitation deficit before 21 LST that increases the PBL temperatures by decreasing the cooling effect of rain evaporation. This warming that persists until dawn certainly plays a key role in the enhancement of the deep convection after 21 LST. During night, the PBL becomes moister in MPHYS with a modest maximum anomaly of 0.3 g kg^{-1} at midnight (the corresponding relative humidity change is negative). The warmer and moister nocturnal PBL, and the larger cloud cover, reinforces also slightly the surface downward longwave flux (up to 2.5 W m^{-2}), which reduces the surface and PBL cooling, leading to a positive surface temperature anomaly of more than 0.3 K at 18 LST. The Aerosol microphysical processes thus reinforce updrafts and precipitation after 21 LST, resulting in larger ice clouds at 15 km. Between 3 and 9 LST, there is a weak reinforcement of the stratiform structure of the vertical wind.

The more obvious radiative effect over the Eastern Region (Figures 9c and 9d) is a large reduction of the upward motion, associated with a modest cooling between 5 and 10 km, with maximum anomaly around midnight. In the morning, the stratiform-type perturbation of the vertical motion is also attenuated by the aerosol radiative effects. The warming between 1 km and 5 km, larger in ABSORB during daylight hours, is mostly related to aerosol absorption of solar radiation but tends to persist day long. The cloud water content decreases above the PBL during day because of the warmer layer and also during night, probably in relation with the deep convection decrease. In ABSORB (FIRE), the PBL is 50 m (10 m) thinner and the surface is 0.5 K (0.2 K) colder in the morning, due to an incident clear-sky solar flux reduced by more than 65 W m^{-2} (39 W m^{-2}) at noon. This indicates weaker vertical mixing in the PBL that explains the drier layer at the PBL top and reinforces the cloudiness dissipation above the PBL in the morning. As proposed by Robock (1988) and examined by Wang and Christopher (2006), this weaker vertical mixing tends to confine aerosols at lower levels. For Borneo, and especially for the drier southern regions, this should increase the aerosol advection toward the SCS in the ABSORB simulation. The persistent moister layer around 2 km in ABSORB is related partly to the larger temperature (i.e., larger saturation water vapor) and partly to a reinforced water vapor convergence induced by synoptic-scale aerosol radiative perturbations discussed below (Figure 12). Because of the small AOD (Figure 2), temperature and moisture perturbations due to aerosol radiative effects are small in the PBL for the Eastern Region for both FIRE and ABSORB. The suppressed convection over the Eastern Region is thus probably related mostly to the perturbation of the synoptic-scale circulation generated by the large-scale aerosol radiative effect, as discussed in section 5.3.

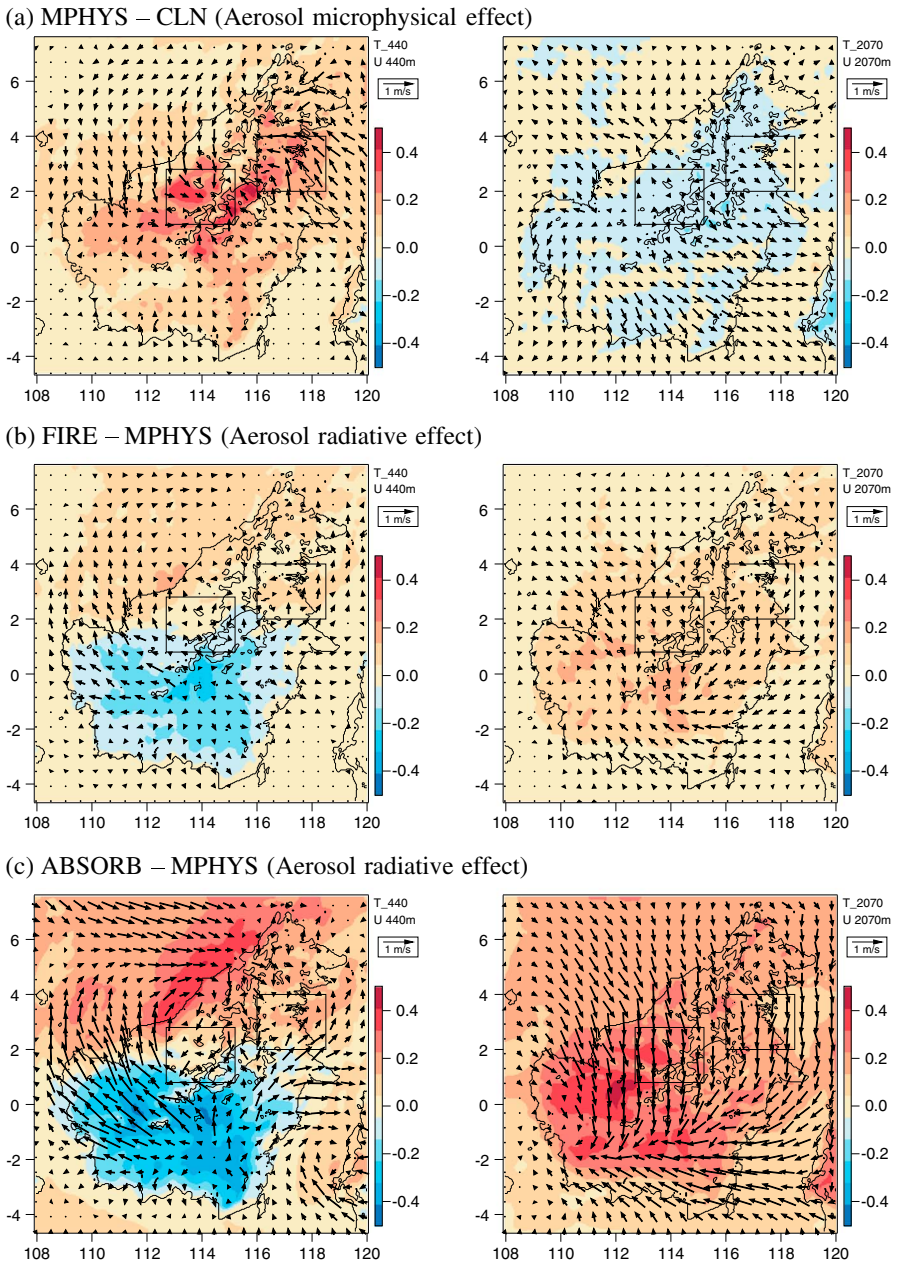

Figure 11. Map of wind and temperature perturbations for model layers at 440 m (left column) and 2,070 m (right column) above the surface for (a) MPHYS-CLN, (b) FIRE-MPHYS, and (c) ABSORB-MPHYS. Wind and temperatures are averaged on model levels for the entire simulation period (23 August to 30 September).

Over the Central Region, radiative aerosol processes increase rainfall with a maximum at 21 LST (Figures 7 and 8d). As stated above, the larger aerosol loading over this region could explain part of this difference with the Eastern Region. For the Central Region, the diurnal evolution of the profiles is discussed only for the aerosol radiative effect in ABSORB, since the microphysical effect is similar to that of the Eastern Region and since the radiative effect is small in FIRE. Aerosol radiative processes give a positive anomaly of the vertical velocity between 15 LST and midnight, associated with a positive anomaly of both liquid and ice clouds. Compared to MPHYS, the PBL in ABSORB is 100 m thinner and the surface is 1.1 K colder in the morning, due to an incident clear-sky solar flux reduced by more than 90 W m^{-2} at noon. Due to the larger aerosol loading, the surface and PBL perturbations are thus exacerbated compared to the Eastern Region. In addition, the temperature warming in the aerosol layer is larger (0.5 K instead of 0.3 K). This contributes to larger

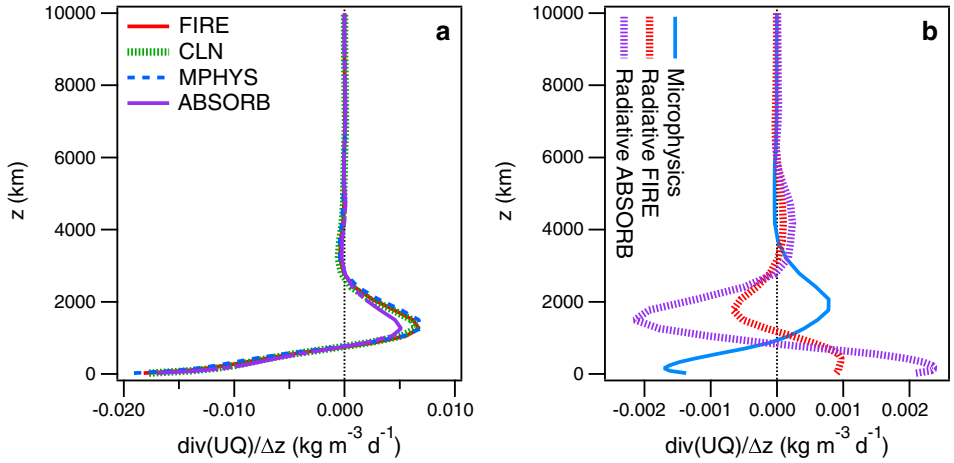

Figure 12. (a) Average water vapor horizontal divergence profiles over the entire Borneo land mass and (b) the corresponding perturbations due to microphysical and radiative effects of smoke aerosols.

low-level cloud dissipation (Figure 10) and smaller rainfall (Figure 8d) between sunrise and 15 LST. This smaller rainfall during the day, the reinforced water vapor in the PBL in the evening (Figure 10), and the reinforced deep convection in early night are consistent with the process proposed by Fan et al. (2015) for mountainous regions. It is, however, difficult to fully explain this reinforcement and other perturbations, like the larger water vapor around 2.5 km, by local processes alone.

5.3. Synoptic-Scale Aerosol Perturbations

Aerosol microphysical processes produce an average surface heating at the island scale (Figure 11a) that generates a low pressure and a low-level wind convergence (possibly reinforced by the deep convection response to the warmer PBL) from the ocean toward the Island. This is mainly due to the warmer surface and boundary layer in the evening that was already discussed for the Eastern Region but that affects most of Borneo Island and especially regions surrounding the mountains. The increased low-level convergence is especially remarkable over the Eastern and the Central Regions that correspond to regions of maximum positive rainfall anomaly due to microphysical processes (Figures 6c and 7 at 5 LST). The low-level wind perturbation is, however, not localized only around the two regions but is a large-scale perturbation affecting the entire domain with a low-level cyclonic vorticity north of the equator. Northerly wind anomalies to the west and southeasterly wind anomalies to the east are also clearly influenced by the coastline and by the orography that generates a discontinuity along the mountain ridge. At an altitude around 2 km, the temperature anomaly is slightly negative and the wind anomaly is rather diverging from the island, showing the shallowness of the dynamical perturbation. The average water vapor divergence profile over the island (Figure 12a) shows convergence below 700 m and a divergence between 700 and 2,500 m for the four simulations. Aerosol microphysical processes increase the water convergence at low level and the divergence around 2,000 m. The average microphysical effect is a slight increase of the divergence of water from the island (+0.09 kg m^{-2} d^{-1}).

The surface and the PBL temperature is reduced south of 2°N in FIRE (Figure 11b) and ABSORB (Figure 11c) compared to MPHYS because of strong aerosol diffusion and absorption of the solar radiation. This is in agreement with Ge et al. (2014). This generates a low-level divergence anomaly over these regions from the south part of the island toward surrounding ocean regions. At 2 km, the warm layer due to aerosol absorption is associated with a convergence anomaly from surrounding ocean regions. This shallow circulation is exacerbated in ABSORB compared to FIRE and may explain the large positive moisture anomaly around 2 km over the Eastern (Figure 9d) and Central (Figure 10) regions. The large low-level divergence over South Borneo transports more aerosols toward the SCS compared to FIRE. This transport is likely enhanced due to larger aerosol concentrations in a more stable PBL (Robock, 1988). Over the SCS, the increased aerosol content is, however, limited to regions near the southwest Borneo coast and can only partially explain the warmer PBL over SCS regions farther north. The low-level divergent circulation anomaly (Figure 11c)

reinforces the average low-level wind (shown on Figure 2) and the surface evaporation (not shown) along the SCS coast. This could explain the larger convective activity over the SCS near the coast during morning hours (Figure 7).

Figure 12b confirms that aerosol radiative processes decrease the convergence of water at low levels and the divergence of water around 2,000 m with a larger effect for ABSORB. This may explain the large water vapor positive anomaly around 2.5 km in ABSORB (Figures 9d and 10). The average radiative effect is a decrease of the convergence of water (+0.25 kg m^{-2} d^{-1}) toward the island in FIRE and an increase of this convergence (−0.42 kg m^{-2} d^{-1}) in ABSORB due to a convergence perturbation around 2 km larger than the divergence perturbation below. Such increased wind convergence due to aerosol radiative effect was also reported in Ge et al. (2014) over the Karimata Strait and southern Borneo.

6. Summary and Discussion

The impact of smoke aerosols on the diurnal cycle of deep convective clouds and precipitation is studied for the tropical island of Borneo during the boreal summer of 2009 using the coupled aerosol-meteorological WRF-Chem model at a cloud-permitting scale of 4 km. The main findings are as follows:

1. WRF captures reasonably well the observed diurnal variation of high cloudiness and rainfall during the boreal summer of 2009.
2. *Combined radiative and microphysical effects* of moderately absorbing fire aerosols (FIRE) decrease the domain average rainfall by 25% at the peak of convective activity (20 LST). Highly absorbing fire aerosols (ABSORB) also decrease the domain average rainfall by 20% in the afternoon but increase it after midnight with a maximum of 15% at 5 LST. This difference shows that aerosol radiative effects depend drastically on the aerosol absorptive properties.
3. For moderately absorbing aerosols (FIRE), *radiative processes* tend to suppress convection over most regions. This suppression may be attributed mostly to local radiative processes that increase the static stability due to the surface cooling and atmosphere warming induced by scattering and absorption of solar radiations by the aerosol layer.
4. For highly absorbing aerosol (ABSORB), radiative processes tend to increase convective rainfall over most oceanic and land regions along the SCS coast by two processes. The increased convection over the oceanic regions is possibly related to increased evaporation caused by the reinforced average circulation generated by the aerosol low-level cooling south of the island (Figure 11c). The nighttime rainfall reinforcement over mountainous regions of Central Borneo is consistent with radiative processes described by Fan et al. (2015). The suppression of the convection over Eastern Borneo by radiative aerosol effect is probably related to the perturbation of the synoptic-scale circulation.
5. Aerosol *microphysical processes* decrease the domain average rainfall with a maximum value of 15% at 21 LST. However, microphysical processes locally increase deep convection at night near the mountains and especially over both Eastern and Central Borneo regions. Cloud liquid water content is maximal near these mountainous regions and locally increases by 30% due to microphysical processes. For these regions, the PBL temperature anomaly is maximal at sunset, which is consistent with reinforced nighttime convection. This PBL temperature anomaly could result from the reduced shallow convection and precipitation in the afternoon caused by reduced cloud droplets collision and coalescence processes. This process is different from that proposed in Fan et al. (2015) because it involves only microphysical processes and it concerns the temperature of the PBL instead of the water content and because the rainfall is enhanced over the valley rather than the mountains.
6. Considering the whole Borneo Island, the aerosol radiative characteristics (their absorptive properties) play a key role in determining the perturbation of the water vapor convergence toward the island. Aerosol radiative processes increase water vapor convergence toward the island in ABSORB and decrease it in FIRE (Figure 12).

As shown in Figures 5 and 8, the generic model response over most regions is mostly a negative rainfall tendency during the day and a positive one during night. This is consistent with the results reported in Wu et al. (2011) and Zhao et al. (2011) showing reduced precipitation, due to increased atmospheric stability in late afternoon, and enhanced nocturnal and early morning precipitation. In Wu et al. (2011) the afternoon decrease is larger than the nighttime enhancement, leading to a net reduction of precipitation mostly due

to aerosol radiative effects and only slightly mitigated by microphysical processes. Our results show that microphysical processes may have a large impact over areas located near the Borneo mountainous region by giving a nighttime rainfall enhancement greater than the afternoon decrease. For these regions, as shown for two selected Eastern and Central Borneo regions, the radiative effect is much more variable in sign, amplitude, and phase and strongly influences the net perturbation of rainfall. As discussed above, these effects are a mixture of local processes and of large-scale processes related to the dynamic response at synoptic scales. The examination of local average diurnal variations and of synoptic maps gives some understanding of the mechanisms explaining the rainfall increase due to aerosol microphysical effects and helps to understand the difference between the FIRE and the ABSORB simulations. However, it does not help to understand the large differences in the rainfall response of the Eastern and the Central Regions to aerosol radiative forcing. This difference could be principally due to the difference in aerosol loading over the two regions or to differences in local circulations induced by the orography and/or the coastline.

Further studies are needed to fully understand the mechanisms of the response of the convection to fire aerosol emissions and in particular to determine more precisely the local impact of aerosol on the static stability compared to synoptic dynamical perturbations of the water vapor convergence. It is also necessary to perform additional regional analyses over ocean regions and more detailed analyses of local diurnal circulations near mountainous regions and near the coastline.

A major result of this study is to show the large sensitivity of rainfall perturbations to aerosol absorptive properties. Aerosol absorption is determined by the amount of highly absorbing constituents such as black and brown carbon relative to other nonabsorbing constituents. Our results imply that an accurate characterization of the composition of biomass burning plumes is key to predicting aerosol/cloud interactions. Such characterization is rarely available from field measurements in complex biomass burning regions (Akagi et al., 2011) such as Borneo where the smoke plume is a mixture of peatland and agricultural burning. A recent field study by Stockwell et al. (2016) reported that smoke aerosols that are emitted from peatland fires over Borneo are moderately absorbing (SSA ~0.958 at 440 nm) due to a very low fraction of black carbon that is present in those emissions. But large uncertainties subsist in terms of optical properties of aged smoke plumes that arrive over the regions of active convection. It is thus necessary to improve our knowledge of these properties by performing more in situ observations of fire aerosols.

Acknowledgments

Authors acknowledge P. Saide (NCAR) for providing the modified WRF-Chem code used in this work, G. Thompson (NCAR) for helpful discussions about his microphysics scheme, A. Teerachai (U. Phayao, Thailand) for preparing input files for WRF simulations, S. Massie (University of Colorado) for help with the extraction of the MODIS data, and J. Fast (PNNL) and A. Gettelman (NCAR) for preforming the NCAR internal review of this manuscript. All the data used within our modeling framework can be obtained from the NCAR data archive available at https://rda.ucar.edu and https://www2.acom.ucar.edu. This research was supported by the National Center for Atmospheric Research, which is operated by the University Corporation for Atmospheric Research on behalf of the National Science Foundation. We would like to acknowledge high-performance computing support from Yellowstone provided by NCAR's Computational and Information Systems Laboratory. A. H. was supported by EPA STAR 83587701-0 and NASA NNX15AE38G. The views expressed in this document are solely those of the authors and do not necessarily reflect those of the Agencies.

References

Akagi, S. K., Yokelson, R. J., Wiedinmyer, C., Alvarado, M. J., Reid, J. S., Karl, T., … Wennberg, P. O. (2011). Emission factors for open and domestic biomass burning for use in atmospheric models. *Atmospheric Chemistry and Physics*, *11*, 4039–4072. https://doi.org/10.5194/acp-11-4039-2011

Albrecht, B. A. (1989). Aerosols, cloud microphysics, and fractional cloudiness. *Science*, *245*, 1227–1230.

Andreae, M. O., Rosenfeld, D., Artaxo, P., Costa, A. A., Frank, G. P., Longo, K. M., & Silva-Dias, M. A. F. (2004). Smoking rain clouds over the Amazon. *Science*, *303*, 1337–1342. https://doi.org/10.1126/science.1092779

Barlage, M., Chen, F., Tewari, M., Ikeda, K., Gochis, D., Dudhia, J., … Mitchell, K. (2010). Noah land surface model modifications to improve snowpack prediction in the Colorado Rocky Mountains. *Journal of Geophysical Research*, *115*, D22101. https://doi.org/10.1029/2009JD013470

Boucher, O., Randall, D., Artaxo, P., Bretherton, C., Feingold, G., Forster, P., … Zhang, X. Y. (2013). Clouds and aerosols. In: Climate change 2013: The physical science basis. In *Contribution of working group I to the fifth assessment report of the intergovernmental panel on climate change*. Cambridge, UK and New York: Cambridge University Press.

DeMott, P. J., Prenni, A. J., Liu, X., Kreidenweis, S. M., Petters, M. D., Twohy, C. H., … Tolbert, M. A. (2010). Predicting global atmospheric ice nuclei distributions and their impacts on climate. *Proceedings of the National Academy of Sciences of the United States of America*, *107*, 11,217–11,222. https://doi.org/10.1073/pnas.0910818107

Duvel, J. P., & Raberanto, P. (2000). A geophysical cross-calibration approach for broadband channels: Application to the ScaRaB experiment. *Journal of Atmospheric and Oceanic Technology*, *17*, 1609–1617.

Emmons, L. K., Walters, S., Hess, P. G., Lamarque, J.-F., Pfister, G. G., Fillmore, D., … Kloster, S. (2010). Description and evaluation of the Model for Ozone and Related chemical Tracers, version 4 (MOZART-4). *Geoscientific Model Development*, *3*, 43–67. https://doi.org/10.5194/gmd-3-43-2010

Fan, J., Leung, L. R., Rosenfeld, D., Chen, Q., Li, Z., Zhang, J., & Jan, H. (2013). Microphysical effects determine macrophysical response for aerosol impacts on deep convective clouds. *Proceedings of the National Academy of Sciences of the United States of America*, *101*(48), E4581–E4590.

Fan, J., Rosenfeld, D., Yang, Y., Zhao, C., Leung, L. R., & Li, Z. (2015). Substantial contribution of anthropogenic air pollution to catastrophic floods in Southwest China. *Geophysical Research Letters*, *42*, 6066–6075. https://doi.org/10.1002/2015GL064479

Ge, C., Wang, J., & Reid, J. S. (2014). Mesoscale modeling of smoke transport over the Southeast Asian Maritime Continent: Coupling of smoke direct radiative effect below and above the low-level clouds. *Atmospheric Chemistry and Physics*, *14*, 159–174. https://doi.org/10.5194/acp-14-159-2014

Grell, G. A., & Freitas, S. R. (2014). A scale and aerosol aware stochastic convective parameterization for weather and air quality modeling. *Atmospheric Chemistry and Physics*, *14*, 5233–5250.

Grell, G., Freitas, S. R., Stuefer, M., & Fast, J. (2011). Inclusion of biomass burning in WRF-Chem: Impact of wild fires on weather forecasts. *Atmospheric Chemistry and Physics*, *11*, 5289–5303.

Hodzic, A., Madronich, S., Bohn, B., Massie, S., Menut, L., & Wiedinmyer, C. (2007). Wildfire particulate matter in Europe during summer 2003: Meso-scale modeling of smoke emissions, transport and radiative effects. *Atmospheric Chemistry and Physics*, *7*, 4043–4064. https://doi.org/10.5194/acp-7-4043-2007

Houze, R. A. (1997). Stratiform precipitation in regions of convection: A meteorological paradox? *Bulletin of the American Meteorological Society*, *78*, 2179–2195.

Huffman, G. J., Adler, R. F., Bolvin, D. T., Gu, G., Nelkin, E. J., Bowman, K. P., … Wolff, D. B. (2007). The TRMM multi-satellite precipitation analysis: Quasi-global, multi-year, combined-sensor precipitation estimates at fine scale. *Journal of Hydrometeorology*, *8*, 38–55.

Iacono, M. J., Delamere, J. S., Mlawer, E. J., Shephard, M. W., Clough, S. A., & Collins, W. D. (2008). Radiative forcing by long-lived greenhouse gases: Calculations with the AER radiative transfer models. *Journal of Geophysical Research*, *113*, D13103. https://doi.org/10.1029/2008JD009944

Iacono, M. J., Mlawer, E. J., Clough, S. A., & Morcrette, J.-J. (2000). Impact of an improved longwave radiation model, RRTM, on the energy budget and thermodynamic properties of the NCAR community climate model, CCM3. *Journal of Geophysical Research*, *105*, 14,873–14,890. https://doi.org/10.1029/2000JD900091

Janhall, S., Andreae, M. O., & Poschl, U. (2010). Biomass burning aerosol emissions from vegetation fires: Particle number and mass emission factors and size distributions. *Atmospheric Chemistry and Physics*, *10*(3), 1427–1439.

Janjić, Z. I. (2002). Nonsingular implementation of the Mellor–Yamada level 2.5 scheme in the NCEP meso model. *NCEP Office note*, *437*, 61.

Kaiser, J. W., Heil, A., Andreae, M. O., Benedetti, A., Chubarova, N., Jones, L., … van der Werf, G. R. (2012). Biomass burning emissions estimated with a global fire assimilation system based on observed fire radiative power. *Biogeosciences*, *9*, 527–554. https://doi.org/10.5194/bg-9-527-2012

Koren, I., Martins, J. V., Remer, L. A., & Afargan, H. (2008). Smoke invigoration versus inhibition of clouds over the Amazon. *Science*, *321*(5891), 946–949. https://doi.org/10.1126/science.1159185

Krueger, S. K., Fu, Q., Liou, K., & Chin, H.-N. S. (1995). Improvements of an ice-phase microphysics parameterization for use in numerical simulations of tropical convection. *Journal of Applied Meteorology*, *34*, 281–287. https://doi.org/10.1175/1520-0450-34.1.281

National Center for Environmental Prediction (2000). NCEP FNL operational model global tropospheric analyses, continuing from July 1999. In *Research data archive at the National Center for Atmospheric Research* (chap. 7, pp. 573–636). Boulder, CO: Computational and Information Systems Laboratory.

Petters, M. D., Carrico, C. M., Kreidenweis, S. M., Prenni, A. J., DeMott, P. J., Collett, J. L. Jr., & Moosmuller, H. (2009). Cloud condensation nucleation activity of biomass burning aerosol. *Journal of Geophysical Research*, *114*, D22205. https://doi.org/10.1029/2009JD012353

Petters, M. D., & Kreidenweis, S. M. (2007). A single parameter representation of hygroscopic growth and cloud condensation nucleus activity. *Atmospheric Chemistry and Physics*, *7*, 1961–1971. https://doi.org/10.5194/acp-7-1961-2007

Phillips, V. T. J., DeMott, P. J., & Andronache, C. (2008). An empirical parameterization of heterogeneous ice nucleation for multiple chemical species of aerosol. *Journal of the Atmospheric Sciences*, *65*, 2757–2783. https://doi.org/10.1175/2007JAS2546.1

Reid, J. S., Hyer, E. J., Johnson, R. S., Holben, B. N., Yokelson, R. J., Zhang, J., … Liew, S. C. (2013). Observing and understanding the Southeast Asian aerosol system by remote sensing: An initial review and analysis for the Seven Southeast Asian Studies (7SEAS) program. *Atmospheric Research*, *122*, 403–468. https://doi.org/10.1016/j.atmosres.2012.06.005

Reid, J. S., Koppmann, R., Eck, T. F., & Eleuterio, D. P. (2005). A review of biomass burning emissions part II: Intensive physical properties of biomass burning particles. *Atmospheric Chemistry and Physics*, *5*, 799–825. https://doi.org/10.5194/acp-5-799-2005

Robock, A. (1988). Enhancement of surface cooling due to forest fire smoke. *Science*, *242*, 911–913.

Rosenfeld, D. (1999). TRMM observed first direct evidence of smoke from forest fires inhibiting rainfall. *Geophysical Research Letters*, *26*, 3105–3108.

Rosenfeld, D., Lohmann, U., Raga, G. B., O'Dowd, C. D., Kulmala, M., Fuzzi, S., … Andreae, M. O. (2008). Flood or drought: How do aerosols affect precipitation? *Science*, *321*, 1309–1313. https://doi.org/10.1126/science.1160606

Ruiz-Arias, J. A., Dudhia, J., & Gueymard, C. A. (2014). A simple parameterization of the short-wave aerosol optical properties for surface direct and diffuse irradiances assessment in a numerical weather model. *Geoscientific Model Development*, *7*, 1159–1174.

Saide, P. E., Thompson, G., Eidhammer, T., da Silva, A. M., Pierce, R. B., & Carmichael, G. R. (2016). Assessment of biomass burning smoke influence on environmental conditions for multiyear tornado outbreaks by combining aerosol-aware microphysics and fire emission constraints. *Journal of Geophysical Research: Atmospheres*, *121*, 10,294–10,311. https://doi.org/10.1002/2016JD025056

Sayer, A. M., Hsu, N. C., Eck, T. F., Smirnov, A., & Holben, B. N. (2014). AERONET-based models of smoke-dominated aerosol near source regions and transported over oceans, and implications for satellite retrievals of aerosol optical depth. *Atmospheric Chemistry and Physics*, *14*, 11,493–11,523. https://doi.org/10.5194/acp-14-11493-2014

Schultz, M., Rast, S., van het Bolscher, M., Pulles, T., Pereira, J., Spessa, A., … Szopa, S. (2007). REanalysis of the TROpospheric chemical composition over the past 40 years, a long-term global modeling study of tropospheric chemistry funded under the 5th EU framework program (Tech. Rep., EU-Contract No. EVK2-CT-2002-00170). Retrieved from http://retro.enes.org/reports/D1-6_final.pdf

Smith, S. J., & Bond, T. C. (2014). Two hundred fifty years of aerosols and climate: The end of the age of aerosols. *Atmospheric Chemistry and Physics*, *14*, 537–549. https://doi.org/10.5194/acp-14-537-2014

Stockwell, C. E., Jayarathne, T., Cochrane, M. A., Ryan, K. C., Putra, E. I., Saharjo, B. H., … Yokelson, R. J. (2016). Field measurements of trace gases and aerosols emitted by peat fires in Central Kalimantan, Indonesia, during the 2015 El Niño. *Atmospheric Chemistry and Physics*, *16*, 11,711–11,732. https://doi.org/10.5194/acp-16-11711-2016

Ten Hoeve, J. E., Jacobson, M. Z., & Remer, L. A. (2012). Comparing results from a physical model with satellite and in situ observations to determine whether biomass burning aerosols over the Amazon brighten or burn off clouds. *Journal of Geophysical Research*, *117*, D08203. https://doi.org/10.1029/2011JD016856

Thompson, G., & Eidhammer, T. (2014). A study of aerosol impacts on clouds and precipitation development in a large winter cyclone. *Journal of the Atmospheric Sciences*, *71*, 3636–3658.

Tosca, M. G., Randerson, J. T., Zender, C. S., Nelson, D. L., Diner, D. J., & Logan, J. A. (2011). Dynamics of fireplumes and smoke clouds associated with peat and deforestation fires in Indonesia. *Journal of Geophysical Research*, *116*, D08207. https://doi.org/10.1029/2010JD015148

Twomey, S. (1977). The influence of pollution on the shortwave albedo of clouds. *Journal of the Atmospheric Sciences*, *34*, 1149–1152.

Wang, J., & Christopher, S. A. (2006). Mesoscale modeling of Central American smoke transport to the United States: 2. Smoke radiative impact on regional surface energy budget and boundary layer evolution. *Journal of Geophysical Research*, *111*, D14S92. https://doi.org/10.1029/2005JD006720

Wang, J., Christopher, S. A., Nair, U. S., Reid, J. S., Prins, E. M., Szykman, J., & Hand, J. L. (2006). Mesoscale modeling of Central American smoke transport to the United States: 1. "Top-down" assessment of emission strength and diurnal variation impacts. *Journal of Geophysical Research*, *111*, D05S17. https://doi.org/10.1029/2005JD006416

Wang, X., Zhang, L., & Moran, M. D. (2010). Uncertainty assessment of current size-resolved parameterizations for below-cloud particle scavenging by rain. *Atmospheric Chemistry and Physics*, *10*, 5685–5705. https://doi.org/10.5194/acp-10-5685-2010

Wiedinmyer, C., Akagi, S. K., Yokelson, R. J., Emmons, L. K., AlSaadi, J. A., Orlando, J. J., & Soja, A. J. (2011). The fire inventory from NCAR (FINN): A high resolution global model to estimate the emissions from open burning. *Geoscientific Model Development*, *4*, 625–641. https://doi.org/10.5194/gmd-4-625-2011

Wu, L., Su, H., & Jiang, J. H. (2011). Regional simulations of deep convection and biomass burning over South America: 2. Biomass burning aerosol effects on clouds and precipitation. *Journal of Geophysical Research*, *116*, D17209. https://doi.org/10.1029/2011JD016106

Yang, G. Y., & Slingo, J. (2001). The diurnal cycle in the tropics. *Monthly Weather Review*, *129*(4), 784–801.

Yu, H., Liu, S. C., & Dickinson, R. E. (2002). Radiative effects of aerosols on the evolution of the atmospheric boundary layer. *Journal of Geophysical Research*, *107*(D12), 4142. https://doi.org/10.1029/2001JD000754

Zhang, Y., Fu, R., Yu, H., Dickinson, R. E., Juarez, R. N., Chin, M., & Wang, H. (2008). A regional climate model study of how biomass burning aerosol impacts land-atmosphere interactions over the Amazon. *Journal of Geophysical Research*, *113*, D14S15. https://doi.org/10.1029/2007JD009449

Zhang, Q., Jimenez, J., Canagaratna, M., Allan, J., Coe, H., Ulbrich, I., … Worsnop, D. R. (2007). Ubiquity and dominance of oxygenated species in organic aerosols in anthropogenically-influenced Northern Hemisphere midlatitudes. *Geophysical Research Letters*, *34*, L13801. https://doi.org/10.1029/2007GL029979

Zhao, C., Liu, X., Ruby, L. L., & Hagos, S. (2011). Radiative impact of mineral dust on monsoon precipitation variability over West Africa. *Atmospheric Chemistry and Physics*, *11*, 1879–1893.